TEM and Laser-Polarized ^{129}Xe NMR Characterization of Oxidatively Purified Carbon Nanotubes

J. M. Kneller,[†] R. J. Soto,[†] S. E. Surber,[†] J.-F. Colomer,[‡] A. Fonseca,[‡] J. B. Nagy,[‡] G. Van Tendeloo,[§] and T. Pietra*β*

Contribution from the Department of Chemistry, New Mexico Tech, Socorro, New Mexico 87801, Laboratoire de Résonance Magnétique Nucléaire, Facultés Universitaires Notre-Dame de la Paix, 61 rue Bruxelles, 5000 Namur, Belgium, and EMAT, University of Antwerp, Groenenborgerlaan 171, B-2020 Antwerp, Belgium

Received December 20, 1999. Revised Manuscript Received August 10, 2000

Abstract: Multiwall carbon nanotubes are produced by decomposition of acetylene at 600 °C on metal catalysts supported on NaY zeolite. The support and the metal are eliminated by dissolving them in aqueous hydrofluoric acid (HF). Two methods were used to eliminate the pyrolitic carbon: oxidation in air at 500 °C and oxidation by potassium permanganate in acidic solution at 70 °C. The progress and efficacy of the purification methods are verified by TEM. The properties of the purified multiwalled carbon nanotubes are probed using ^{13}C and ^{129}Xe NMR spectroscopy under continuous-flow optical-pumping conditions. Xenon is shown to penetrate the interior of the nanotubes. A distribution of inner tube diameters gives rise to chemical shift dispersion. When the temperature is lowered, an increasing fraction of xenon resides inside the nanotubes and is not capable of exchanging with xenon in the interparticle space. In the case of the permanganate-oxidized sample, rapid xenon relaxation is attributed to interaction with residual MnO_2 nanoparticles in the interior of the tubes.

Introduction

Since their discovery,[1] carbon nanotubes have promised a multitude of applications, due to their molecular structure and their electronic and mechanical properties. The two well-known forms of crystalline carbon, the sp^3-bonded diamond, an insulator with a gap too large for most applications, and the sp^2-bonded graphite, a semi-metal, have limited use. A nanotube can be constructed by wrapping up a single graphene sheet such that two equivalent sites of the hexagonal lattice coincide. This roll-up quantizes the momentum of the electrons moving around the periphery of the tube. As a result, the tubes are either one-dimensional metals or semiconductors, depending on how the momentum value correlates with the preferred direction for conduction of electrons.[2] The multiwall nanotube structure is typically turbostratic; each concentric graphitic layer can have a different orientation. Their gas adsorption capabilities give carbon nanotubes potential both as gas storage media[3] and as gas sensors.[4,5] A hydrogen storage capacity of 0.52 hydrogen/carbon could be achieved at room temperature under moderate pressure (10 MPa),[3] while the adsorption of NO_2 and NH_3 led to a significant change in conductance.[4] The adsorption of oxygen on single-wall carbon nanotubes not only changed their conductivity but also affected thermopower and local density of states, suggesting that fundamental studies of nanotube properties be carried out under careful control of the environment.[5] In this work, xenon sorption properties of carbon nanotubes synthesized by catalytic decomposition of acetylene and then purified by oxidation in air or with potassium permanganate are studied with ^{129}Xe nuclear magnetic resonance (NMR) spectroscopy. The oxidative purification takes advantage of the reactivity difference between carbon nanotubes and carbon nanoparticles or pyrolitic carbon, which have a different three-dimensional structure. Using continuous-flow optical-pumping ^{129}Xe NMR spectroscopy, we show that these different oxidizing agents change the properties of the carbon nanotubes.

NMR of ^{129}Xe has proven to be an effective tool for the characterization of microporous materials;[6−9] however, limitations in signal intensity arise due to the low spin density of a gas under thermal equilibrium conditions. In recent years, techniques for the enhancement of the NMR signal using laser-polarized gases such as ^{3}He and ^{129}Xe have been developed.[10−12] With high-power laser diode arrays, a continuous flow of optically polarized xenon can be generated and circulated over the sample surface.[13] This technique has been applied in the present work.

[†] New Mexico Tech.
[‡] Universitaires Notre-Dame de la Paix.
[§] University of Antwerp.

(1) Iijima, S. *Nature* **1991**, *354*, 56−58.
(2) Dresselhaus, M. S.; Dresselhaus, G.; Saito, R. *Phys. Rev. B* **1992**, *45*, 6234−6242.
(3) Liu, C.; Fan, Y. Y.; Liu, M.; Cong, H. T.; Cheng, H. M.; Dresselhaus, M. S. *Science* **1999**, *286*, 1127−1129.
(4) Kong, J.; Franklin, N. R.; Zhou, C.; Chapline, M. G.; Peng, S.; Cho, K.; Dai, H. *Science* **2000**, *287*, 622−625.
(5) Collins, P. G.; Bradley, K.; Ishigami, M.; Zettl, A. *Science* **2000**, *287*, 1801−1804.
(6) Barrie, P. J.; Klinowski, J. *Prog. NMR Spectrosc.* **1992**, *24*, 91−108.
(7) Dybowski, C.; Bansal, N.; Duncan, T. *Annu. Rev. Phys. Chem.* **1991**, *42*, 433−464.
(8) Raftery, D.; Chmelka, B. F. In *Solid State NMR I: Methods*; B. Blümich, Ed.; Springer-Verlag: Heidelberg, 1994; Vol. 30, pp 111−158.
(9) Ratcliffe, C. I. In *Annual Reports on NMR Spectroscopy*; G. A. Webb, Ed.; Academic Press: San Diego, 1998; Vol. 36, pp 123−221.
(10) Happer, W.; Miron, E.; Schaefer, S.; Schreiber, D.; van Wijngaarden, W. A.; Zeng, X. *Phys. Rev. A* **1984**, *29*, 3092−3110.
(11) Raftery, D.; Long, H.; Meersmann, T.; Grandinetti, P. J.; Reven, L.; Pines, A. *Phys. Rev. Lett.* **1991**, *66*, 584−587.
(12) Pietrass, T. *Magn. Reson. Rev.* **2000**, *17*, 263−337.
(13) Seydoux, R.; Pines, A.; Haake, M.; Reimer, J. A. *J. Phys. Chem. B* **1999**, *103*, 4629−4637.

10.1021/ja994441y CCC: $19.00
Published on Web 10/14/2000

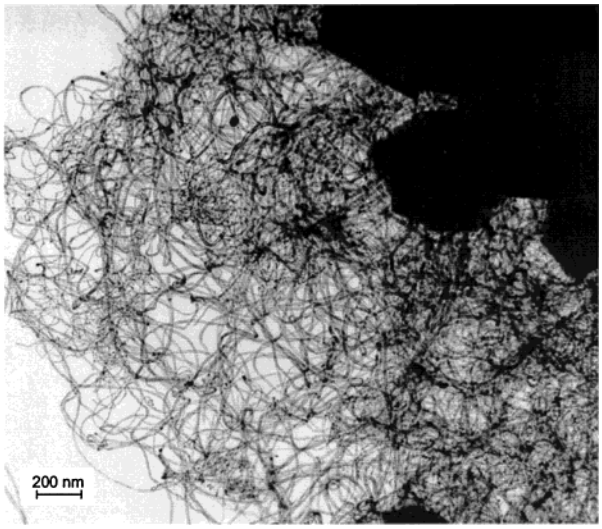

Figure 1. Low-resolution TEM image of multiwall nanotubes produced by decomposition of acetylene at 600 °C on 2.5% Co/zeolite NaY without further purification. The dark area in the top right corner is due to zeolitic support.

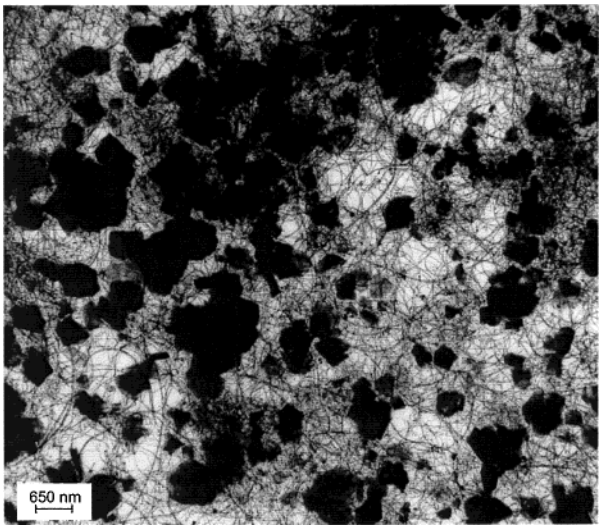

Figure 2. Low-resolution TEM image of the MWNTs sample after HF treatment, showing the high amount of pyrolitic carbon (dark spots).

Experimental Section

Nanotube Synthesis. Multiwalled carbon nanotubes were produced by catalytic decomposition of acetylene over supported catalyst Co/zeolite NaY containing about 2.5 wt % of metal. Complete description of the synthesis method is described in ref 14. The multiwalled carbon nanotubes so produced are characterized by transmission electron microscopy (TEM) to show the good quality (Figure 1) and distribution of diameters.

Purification Process. Dissolution by HF fully removed the zeolitic support. However, the presence of aggregates of pyrolitic carbon is shown by the dark spots in the TEM image (Figure 2). Thus, oxidation is necessary to remove pyrolitic carbon from the carbon nanotubes. Oxidation of carbon in air to carbon monoxide and dioxide occurs if the temperature is sufficiently high (773 K). Oxidation by $KMnO_4$ in acidic solution at 343 K removes the pyrolitic carbon by the generation of carbon dioxide. A complete description of the purification treatments is given in ref 14. Pure carbon nanotubes can be obtained in a 27% or 40% yield after air or permanganate oxidation, respectively (Figure 3). TEM (Philips CM 20 and JEOL CX 200) images of both samples

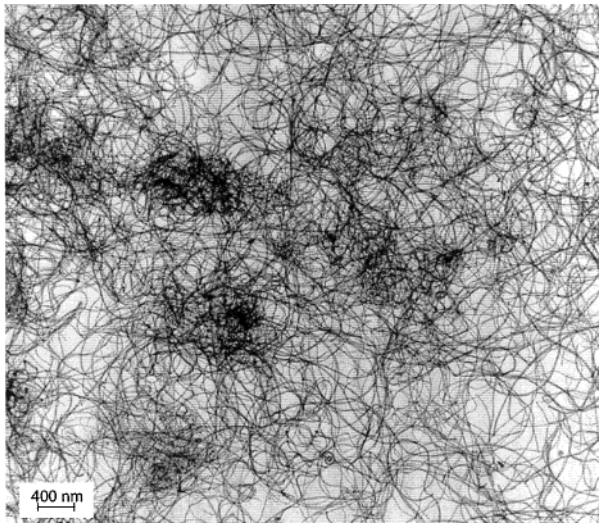

Figure 3. Typical low-resolution TEM image of multiwall carbon nanotubes that were purified by dissolution in HF, followed by oxidation in acidic permanganate solution.

show, on average, 15 graphitic layers, with inner and outer diameters of 6 and 16 nm.[14]

Sample Preparation. About 0.05 g each of the nanotubes oxidized with $KMnO_4$ or in air were tightly packed into the NMR tube and held in place with cleaned glass wool. To remove adsorbed water, the samples were heated under $N_{2(g)}$ flow to 673 K over a period of 2.5 h, kept at this temperature for 2.5 to 6 h, and cooled to ambient temperature. The entire system was evacuated to 1.3 Pa prior to loading pressures from 138 to 525 kPa of the gas mixture (2.24% nitrogen, 8.9% xenon, 88.86% helium). An additional sample of 0.018 g nanotubes oxidized in air was heated to 673 K overnight under vacuum, loaded with pure xenon gas and then flame-sealed. The equilibrium density, determined from the ^{129}Xe NMR chemical shift of xenon in the free gas space, was 21.9 amagat at ambient temperature.[15]

Optical-Pumping Apparatus. The continuous-flow optical-pumping apparatus, similar to the one used by Seydoux et al.,[13] was set up in the fringe field of the superconducting NMR magnet (9.4 T). A fiber-coupled laser diode array (OPTO−Power Corp., Tucson, AZ) delivering 45 W at 795 nm and operating at a current of 28 A was used for the excitation of rubidium. Circular polarization of the pumping light was achieved using a polarizing beam splitter, half-wave and quarter-wave plates (Newport Corp., Irvine, CA). The sample cell (10 mm outer diameter, 8 mm inner diameter) was connected to the optical-pumping setup through the length of the home-built NMR probe with 1.65 mm inner diameter PFA (perfluoro alkoxy, Swagelok) tubing using compression fittings. A few drops of Rb metal were placed in the optical-pumping cell and heated by a stream of hot air to approximately 448 K. Gas flow rates were optimized individually for highest signal intensity. ^{129}Xe NMR spectra of the sample oxidized in air were recorded at a flow rate $j_1 = 0.58 \pm 0.06$ mL/s, while a higher rate, $j_3 = 2.6 \pm 0.3$ mL/s was used for the sample oxidized with permanganate.[16]

NMR experiments were carried out on a Bruker MSL 400 NMR spectrometer operating at a Larmor frequency of 110.668 MHz for ^{129}Xe and 100.613 MHz for ^{13}C. A typical $\pi/2$ pulse duration was 25 μs. Low temperatures were achieved by flowing pre-cooled nitrogen gas through the dewared sample region. For practical reasons, the coil was located slightly off-center in the bore of the magnet. The residual magnetic field inhomogeneity after shimming gave rise to a line width of 150 Hz for xenon gas in an empty sample tube.

(14) Colomer, J. F.; Piedigrosso, P.; Willems, I.; Journet, C.; Bernier, P.; Tendeloo, G. V.; Fonseca, A.; B.Nagy, J. *J. Chem. Soc., Faraday Trans.* **1998**, *94*, 3753−3758.

(15) Jameson, C. J.; Jameson, A. K.; Cohen, S. M. *J. Chem. Phys.* **1973**, *59*, 4540−4546.

(16) Kneller, J. M.; Soto, R. J.; Surber, S. E.; Pietraβ, T.; Colomer, J.-F.; Fonseca, A.; B.Nagy, J. *J. Magn. Reson.* In press.

Results

The catalytic decomposition of acetylene on NaY zeolite-supported Co catalyst led to large production of multiwalled carbon nanotubes.[14−17] The quality of the nanotubes, i.e., the presence of pyrolitic carbon and defect groups, the inner and outer tube diameter, and the length of the tubes, depends on the reaction conditions used: the cobalt content, the reaction temperature, the flow rates of reactants and carrier gas, and the reaction time.

Figure 1 illustrates the low-resolution electron microscope image of an unpurified sample. A rather high density of nanotubes is clearly seen. The dark areas in the image are caused by pyrolitic carbon and the zeolite support. The catalytic support with the metal ions is removed by dissolution in aqueous HF. Unfortunately, a rather high amount of pyrolitic carbon is freed during the removal of the support, suggesting that the pyrolitic carbon was essentially formed inside the zeolitic crystallites (Figure 2). The pyrolitic carbon can be eliminated by selective oxidation with oxygen or an acidic solution of $KMnO_4$. Figure 3 shows that the final carbon nanotubes are quite pure, free of both support and amorphous carbon.

The high quality of the samples was confirmed by high-resolution TEM images of carbon nanotubes produced at 600, 700, and 800 °C. No pyrolitic carbon was formed by pyrolitic decomposition of acetylene at 600 °C. At 700 °C, the presence of pyrolitic carbon sticking to the external wall of the nanotubes is easily identified. Finally, at 800 °C, a large amount of pyrolitic carbon was detected. The effect of the acetylene flow rate shows that amorphous carbon starts to deposit when that flow rate is higher than 15 mL/min. The optimal flow rate is 10 mL/min, which allows a 99% acetylene conversion and a carbon deposit of 20 wt % on the supported catalyst. To summarize, the optimal conditions for the synthesis of carbon nanotubes on NaY-supported Co catalyst for 3.5 g of catalyst with 2.5 wt % of Co are acetylene flow rate, 10 mL/min; nitrogen (carrier gas) flow rate, 110 mL/min; reaction time, 60 min; and reaction temperature, 600 °C. More than 600 mg of deposited carbon could be obtained in each experiment, that is, in 90 min, including both preparation and reaction time. The samples investigated in this work were synthesized under these optimized conditions.

The oxidative purification of carbon nanotubes introduces defect groups such as −COOH, −OH, and carbonyl groups. For the $KMnO_4$ oxidized sample, 0.19 mmol/g carboxyl, 0.79 mmol/g hydroxyl, and 0.76 mmol/g carbonyl were found, while the air-oxidized sample yielded 0.38 mmol/g carboxyl and 0.75 mmol/g hydroxyl. Kuznetsova et al. showed that heating above 580 K under vacuum removes these groups, facilitating entry into the tubes by gas molecules.[18]

Oxidation leads to the opening of the nanotubes as illustrated in Figure 4. Gases can adsorb both in the inner channel of the nanotubes and between them.[18] Because ^{129}Xe NMR is currently used to probe the void space in microporous materials, it is interesting to test the gas sorption properties of carbon nanotubes by using optically polarized xenon. Using this technique, even a small amount of xenon can be detected.

Temperature-dependent ^{129}Xe NMR spectra for both samples are shown in Figure 5a (oxidized in air) and b (oxidized with potassium permanganate). These spectra were obtained under continuous flow optical-pumping conditions. For the sample that was oxidized in air, the signal corresponding to xenon in the adsorbed phase was much stronger at ambient temperature, and its intensity remained roughly constant when the temperature was lowered. Conversely, the corresponding signal was very weak for the sample that was oxidized with permanganate but gained significantly in intensity at lower temperatures. Circulating the gas mixture over the sample at different flow rates affects both chemical shifts and signal build-up rates. These effects were studied in detail for the carbon nanotube sample that was purified with potassium permanganate.[16] The line width of the peak corresponding to xenon in the adsorbed phase increased with decreasing temperature to an extent depending on the flow rate. The most pronounced effect was observed for the highest flow rate, and the largest line width was observed under static conditions (no flow). The chemical shift for xenon in the gas and adsorbed phases is independent of pressure within experimental error in the range of 138 to 483 kPa, which is due to the very low partial pressure of xenon in the mixture (1.43 kPa at a total pressure of 414 kPa).

The ^{129}Xe NMR chemical shifts for xenon in the three phases (gas, adsorbed, and solid) for both samples are summarized in Figure 6 as a function of temperature. The data shown have been corrected for the altered sample temperature that was caused by the gas flow. The temperature calibration was performed in the range between 133 K and 298 K. At flow rate j_3, the warm xenon mixture gas stream led to a temperature

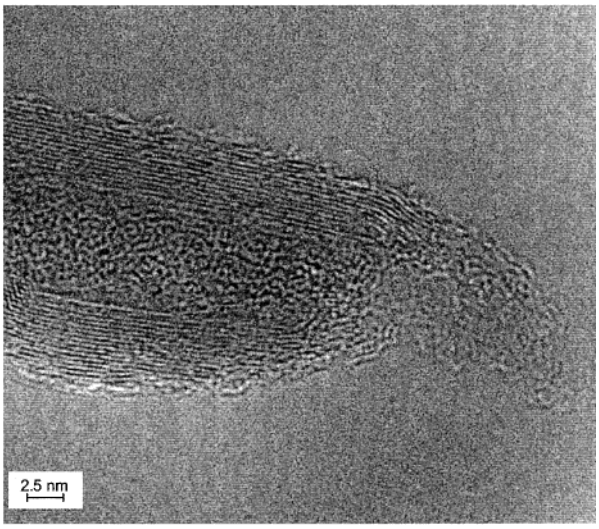

Figure 4. Typical high-resolution TEM image of an uncapped multiwall nanotube.

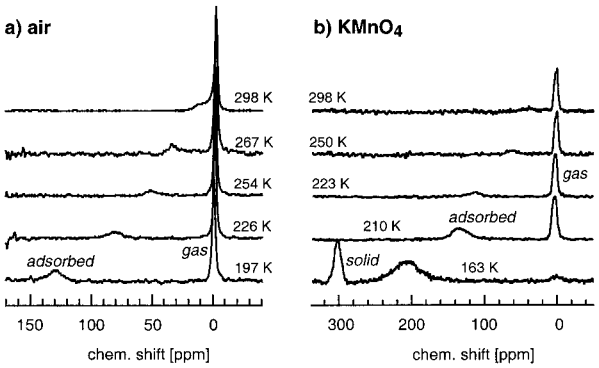

Figure 5. Temperature-dependent ^{129}Xe NMR spectra of xenon adsorbed onto carbon nanotubes (a) purified in air at flow rate j_1, and (b) oxidized with $KMnO_4$ at flow rate j_3. All spectra shown in (a) were recorded with 64 scans. The spectra shown in (b) at 298 and 163 K were recorded with 512 scans, at 202 K with 256 scans, and at 218 and 250 K with 128 scans.

(17) Piedigrosso, P.; Konya, Z.; Colomer, J.-F.; Fonseca, A.; Tendeloo, G. V.; Nagy, J. B. *J. Phys. Chem. Chem. Phys.* **2000**, *2*, 163−170.

(18) Kuznetsova, A.; Yates, J. T., Jr.; Liu, J.; Smalley, R. E. *J. Chem. Phys.* **2000**, *112*, 9590−9598.

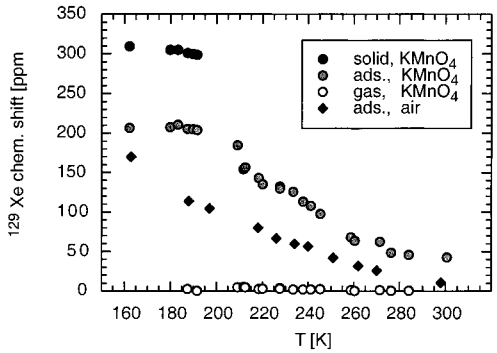

Figure 6. Temperature-dependent ^{129}Xe NMR chemical shifts of gaseous, adsorbed, and solid xenon for carbon nanotubes purified with $KMnO_4$ (circles) obtained at flow rate j_1 and of xenon adsorbed onto nanotubes in air (diamonds) at flow rate j_3. Error bars (±3 ppm) are equal or smaller in size than the symbols. Sample temperatures have been calibrated using the ^{207}Pb NMR chemical shift of lead nitrate.

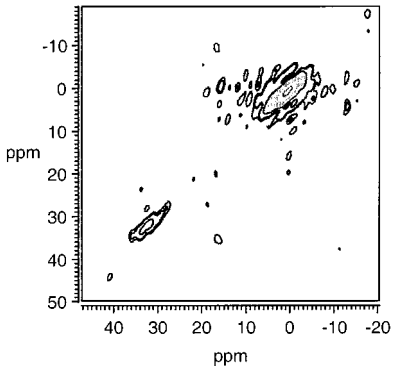

Figure 7. Two-dimensional exchange ^{129}Xe NMR spectrum of xenon in contact with the permanganate-oxidized sample at ambient temperature under thermal equilibrium conditions with a mixing time of 1 ms. The spectrum was recorded with 10 000 scans per free induction decay at a gas pressure of 414 kPa, corresponding to a xenon partial pressure of 1.43 kPa.

increase of the sample.[16] With decreasing temperature, the chemical shifts of physisorbed xenon increased in both samples. For the permanganate-oxidized sample, the shifts moved increasingly downfield as the temperature was lowered as compared to the air-oxidized sample. For the former sample, the chemical shift of xenon in the adsorbed phase reached a limiting value of about 206 ppm below a temperature of 150 K. This was accompanied by the onset of solid xenon formation where Xe−Xe interactions become the dominating contribution to the chemical shift.

Two-dimensional exchange NMR was used to study the exchange dynamics between xenon in the different phases. For the permanganate-oxidized sample and mixing times up to 10 ms at 298 K and 1 ms at 213 K, no cross-peaks were observable between the two resonances (see Figure 5). A typical spectrum recorded at ambient temperature under equilibrium conditions with a mixing time of 1 ms is shown in Figure 7. The equivalent experiment for the air-oxidized sample was not conclusive, due to the much lower signal-to-noise ratio. For the flame-sealed sample, however, very faint cross-peaks were observable for a mixing time of 300 ms at 215 K. Under continuous-flow optical-pumping conditions, very long recycle delays (about 4−5 xenon dwell times in the coil region) were necessary in a two-dimensional experiment to ensure complete gas exchange in the coil region. Due to the short relaxation time of xenon in the adsorbed phase, the spectra gave rise to an overall poorer signal-to-noise ratio at ambient temperature.

^{13}C and ^{129}Xe spin−lattice relaxation times, T_1, under equilibrium conditions were determined for the two samples. The values are listed in Table 1. Because of the weak ^{129}Xe NMR signal intensity under equilibrium conditions for the sample oxidized in air, the temperature dependence of T_1 was investigated using the sample with higher xenon density. Although here within experimental error T_1 was constant for the downfield resonance (ca. 2 s) in the temperature range from 295 to 170 K, T_1 of the gas-phase resonance varied from 9 to 4.5 s and reached its minimum around 255 K. The effect of temperature on chemical shifts and signal intensities for this sample is shown in Figure 8.

^{13}C NMR spectra revealed a single resonance, which narrowed upon magic angle spinning. Signal enhancement exploiting the spin polarization-induced nuclear Overhauser effect[19] was not feasible in a reasonable amount of time, due to the low ^{13}C signal-to-noise ratio.

Discussion

1. Relaxation. The much shorter ^{129}Xe NMR relaxation time for the sample oxidized with permanganate (Table 1) is likely due to paramagnetic effects because the magnetic susceptibility of this sample was 6.1×10^{-8} (at ambient temperature), but only a small degree of diamagnetism (-3.0×10^{-10}) was observed for the sample oxidized in air. There are three possible causes for the paramagnetism observed: defects in the graphitic layers, dangling bonds at the ends of the nanotubes caused by removal of the fullerene half spheres, or residual paramagnetic Mn(IV). Defects were present in both samples to a similar extent, as is evident from the electron micrographs. Dangling bonds are also expected to be formed to a similar extent in both samples. The acidic wash conditions should saturate the dangling bonds in the permanganate-oxidized sample and would give rise to the opposite trend in chemical shifts. Hence, the paramagnetism was most likely caused by residual Mn(IV). Indeed, some 0.01 wt % of manganese was detected by PIXE (depth of analysis, ca. 1 μm). Unfortunately, the XPS technique is much less sensitive (depth of analysis, ca. 50 Å) and only an upper limit could be detected, which was 0.1 wt % of manganese. Because the permanganate-oxidized sample was carefully washed after the oxidation procedure, it is conceivable that Mn(IV) ions were occluded inside the nanotubes as MnO_2 nanoparticles. The interior sites are harder to penetrate with water due to capillary action and are more likely to retain MnO_2. Similarly, it has been shown that metal atoms or clusters may be embedded in the interior of single-walled carbon nanotubes during the growth process and are not completely removed by boiling in 70% nitric acid.[20] However, these results alone do not enable us to situate the MnO_2 conclusively either in the interior only or in both the interior and exterior of the nanotubes.

Further indirect evidence is provided by xenon adsorption and desorption experiments on single-walled carbon nanotubes, which showed that oxidative treatment followed by heating under vacuum significantly increased the nanotubes' sorption capacity and enhanced the rate of xenon capture, due to entry of the gas into the interior of the tubes.[18] The saturation coverage (expressed in xenon atoms per carbon atoms, N_{Xe}/N_C) at 95 K increased by a factor of 12 after oxidation and heating to 623 K, whereas an increase by a factor of 280 to $N_{Xe}/N_C = 0.042$ was achieved when the heating temperature was raised to 1073

(19) Navon, G.; Song, Y.-Q.; Rõõm, T.; Appelt, S.; Taylor, R. E.; Pines, A. *Science* **1996**, *271*, 1848−1851.

(20) Dujardin, E.; Meny, C.; Panissod, P.; Kintzinger, J.-P.; Yao, N.; Ebbesen, T. W. *Solid State Commun.* **2000**, *114*, 543−546.

Table 1: ^{129}Xe and ^{13}C NMR Spin−Lattice Relaxation Times for Carbon Nanotubes Oxidized in Air and with Potassium Permanganate[a]

nucleus	sample	phase	T_1 at 298 K [s]	T_1 at 213 K [s]	T_1 at 166 K [s]
^{129}Xe	$KMnO_4$	gas	0.018 ± 0.002	0.04 ± 0.01	0.13 ± 0.04
		adsorbed	0.010 ± 0.001	0.007 ± 0.001	0.0035 ± 0.0004
	air	gas and adsorbed	4.2 ± 0.4		
^{13}C	$KMnO_4$		1.3 ± 0.3		
	air		6.4 ± 1.5		

[a] The pressure of the gas mixture was 414 kPa for the sample oxidized with permanganate and 511 kPa for the sample oxidized in air. Low-temperature T_1's are not available for the sample oxidized in air, due to apparatus constraints.

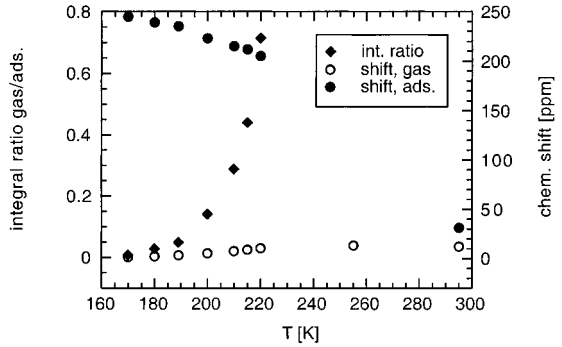

Figure 8. ^{129}Xe NMR chemical shifts and intensity ratios in dependence of temperature for a sample of air-oxidized carbon nanotubes at a xenon density of 21.9 amagat. Unfilled circles correspond to the shifts of the gas-phase resonance; filled circles, to shifts of the adsorbed phase resonance; and diamonds represent ratios of integrated signal intensities of the gas phase over the adsorbed phase resonance. Error bars are smaller than the size of the symbols.

K.[18] We can roughly estimate the saturation coverage from the chemical shift of the gas-phase resonance, which is related to density,[15] to $N_{Xe}/N_C = 0.3$. This larger value may be attributed to easier access to the interior of the nanotubes, due to the much larger tube diameters and, hence, wider openings. Therefore, we expect that in our samples, an increasingly large fraction of the xenon is located inside the nanotubes as the temperature is lowered. This trend can be followed by monitoring the signal intensities of the two resonances under equilibrium conditions (Figure 8). Because paramagnetic Mn(IV) provides an efficient relaxation pathway for xenon (Table 1), and this effect becomes more pronounced as the temperature is lowered, we conclude that the MnO_2 particles must also be located inside the nanotubes.

The ^{13}C T_1's were of the same order of magnitude for both samples, but still slightly shorter for the sample that was oxidized with permanganate (Table 1), indicating that paramagnetic relaxation does not seem to play the same role for ^{13}C as it does for ^{129}Xe. Only a very small fraction of the ^{13}C NMR signal was due to carbon atoms located in close proximity to MnO_2. Due to the large length-to-diameter ratio, these carbon atoms are far outnumbered by the carbon atoms situated further away. Relaxation due to interaction with paramagnetic species falls off with r,[6] where r is the distance between the nuclear spin and the paramagnetic site.[21]

Given the upper limit of the average density of paramagnetic Mn(IV) sites in the material (1.8×10^{-5} Å^{-3}) and a lower limit of the electron relaxation time of 1 ns, a lower limit for the nuclear $T_1 = 100$ s that was due to interaction with paramagnetic sites is estimated.[21] This approximation neglects both the mobility of the xenon and the possibly uneven distribution of Mn(IV) sites (clustering) in the material. For ^{129}Xe, the estimated T_1 differs from the experimental value by 4 orders of magnitude. Because even in the air-oxidized sample, the ^{13}C T_1 was significantly shorter, another mechanism must contribute to relaxation. A possible contribution may arise from interaction with conduction electrons,[22] as recently shown for ^{13}C NMR of single-walled carbon nanotubes.[23] Here, the biexponential magnetization decay was attributed to signal components arising from metallic and semiconducting nanotubes with T_1's in the range of 8−12 s and 52−99 s, respectively, depending on sample preparation.[23] The linear dependence of the reciprocal ^{129}Xe NMR T_1 on temperature for our permanganate-oxidized sample also indicates a Korringa-like contribution to relaxation. No such dependence was observed for the gas-phase resonance or either of the resonances in the air-oxidized sample. For the flame-sealed sample, T_1 of xenon in the adsorbed phase was independent of temperature, which may, however, be attributed to the much higher xenon concentration.

2. Chemical Shifts. The presence of paramagnetic MnO_2 particles will affect not only the ^{129}Xe NMR relaxation times, but also the chemical shifts. A higher chemical shift is expected for the paramagnetic sample, in agreement with the experimental results (Figure 6). It is conceivable that the presence of MnO_2 inside the nanotubes would also decrease the free space available to the xenon and, thus, further augment the shift. Yet, the low concentration of manganese (less than 0.1%) makes it unlikely that such a shift would be detectable. The interaction with paramagnetic species, in contrast, is much stronger and long-ranging and will, thus, have a noticeable effect on chemical shifts.

The difference in the ^{129}Xe chemical shift for xenon in the adsorbed phase for the two samples was most likely caused by the interaction with paramagnetic species present in the $KMnO_4$-oxidized sample. This interaction is expected to increase as the xenon mobility is reduced when the temperature is lowered, which is consistent with the experimental results (Figure 6). ^{129}Xe chemical shifts for xenon physisorbed on chemically comparable systems such as fullerenes under similar experimental conditions are much lower. For C_{60}, a ^{129}Xe NMR chemical shift of about 100 ppm at a temperature of 150 K was observed, and for C_{70}, the shift was about 125 ppm.[24] The chemical shift of xenon in a confined space is predicted to increase when the temperature is lowered unless the pores are very small, that is, on the order of the diameter of a xenon atom.[25] In our case, even the narrowest pores were significantly larger than a xenon atom (30 Å vs 4.4 Å), and the observed trend was expected for xenon dwelling preferentially in the interior of the tubes.

3. Dynamics. The mobility of the xenon may cause it to sample different environments on the NMR time scale, yielding

(21) Abragam, A. *The Principles of Nuclear Magnetism*; Clarendon Press: Oxford, 1989.

(22) Becerra, L. R.; Slichter, C. P.; Sinfelt, J. H. *Phys. Rev. B* **1995**, *52*, 11457−11461.

(23) Tang, X.-P.; Kleinhammer, A.; Shimoda, H.; Fleming, L.; Bennoune, K. Y.; Sinha, S.; Bower, C.; Zhou, O.; Wu, Y. *Science* **2000**, *288*, 492−494.

(24) Brunner, E.; Haake, M.; Pines, A.; Reimer, J. A.; Seydoux, R. *Chem. Phys. Lett.* **1998**, *290*, 112−116.

(25) Cheung, T. T. P. *J. Phys. Chem.* **1995**, *99*, 7089−7095.

average chemical shifts weighted by the xenon's dwell time in the various locations. Therefore, it is possible that the observed chemical shifts present an average of xenon dwelling on the interior and exterior adsorption sites of the nanotubes. This possibility was probed using two-dimensional exchange NMR spectroscopy.[26] For an interpretation of these results, it is necessary to first make an assignment of the two resonances.

In a microcrystalline sample, the xenon NMR signal can arise from different sample regions: the xenon atoms in the overhead gas (reservoir I), xenon in the interparticle space (reservoir II), xenon inside the crystallites within an exchangeable layer surrounding the crystallites (reservoir III), and xenon atoms deep inside the crystal (reservoir IV).[27] Although in the limit of very large crystals, only reservoirs I and IV are effective, for a fine powder, only reservoirs II and III need to be considered.[27] The electron micrographs show that the nanotubes do not form aggregates, but remain separate (Figure 3). Thus, it is necessary to consider all four regions, because the nanotubes are very long (limit of large crystals) but also very thin (limit of a fine powder). For xenon atoms in reservoir II, exchange with xenon in reservoir III is expected.[28] The signal from xenon in the interparticle space will present an average of the chemical shifts of xenon in reservoirs II and III, weighted by the average dwell times in those regions. For a dominating residence time in reservoir II, the average chemical shift should more closely resemble that of the free gas. Therefore, the question arises whether the upfield resonance observed is due to xenon in reservoir I or II.

For the low xenon density samples, we observed that the chemical shift of the upfield resonance was equal for both samples and effectively zero due to the very low partial pressure of xenon (1.43 kPa). Within experimental error (about 1 ppm line width, due to field inhomogeneity), the shift of the upfield resonance was not affected by the presence of the carbon nanotubes. It is also noteworthy that this resonance did not shift downfield when the temperature was lowered. Furthermore, different spin−lattice relaxation times for the two xenon resonances (Figure 5b) of the sample oxidized with permanganate were observed. While the T_1 of physisorbed xenon decreased as the temperature was lowered, the opposite was true for the T_1 of the upfield resonance. If the latter originated from xenon in a typical reservoir II, the same trend in T_1 would have been expected as that for physisorbed xenon, due to the increased contact time with the sample at lower temperatures. Under optical-pumping conditions, it is possible that, due to the large nonequilibrium nuclear spin polarization, this ^{129}Xe resonance could have been picked up from a region not enclosed by the NMR coil (reservoir I), that is, from the region of the glass wool plugs which held the sample in place. However, this resonance was also observed under equilibrium conditions, which makes this assignment unlikely. For the higher density flame-sealed sample, the region containing the sample extended beyond the pick-up coil, so that the gas-phase resonance must have originated from xenon in the interparticle space (reservoir II).

Because reservoir II is capable of exchange with reservoir III, the assignment of the downfield resonance to either reservoir III or IV must be considered. Xenon adsorbed on the exterior of the nanotubes or in their interior in the vicinity of the tube openings corresponds to reservoir III, whereas xenon deep inside the nanotubes represents reservoir IV. Due to the large length-to-diameter ratio of the nanotubes, the number of sites in proximity of the nanotube openings is outnumbered by those on the interior and exterior walls.

The ^{129}Xe NMR chemical shift of the gas-phase resonance in the high-pressure sample experienced an upfield shift as the temperature was lowered, which is due to the decrease in density as more xenon moves into the adsorbed phase (Figure 8). Moreover, the chemical shift of the upfield resonance was exactly equal to that of xenon in the free-gas space above the sample (obtained by turning the sample tube upside down). In addition, the spin−lattice relaxation times of both resonances differed significantly and showed a contrasting temperature dependence. Because the upfield resonance displayed a density-dependent minimum in T_1, it is conceivable that the spin-rotation interaction contributed to relaxation as in free xenon gas.[29] All of these facts point to weak communication between the two reservoirs, which stands in stark contrast to the large and highly temperature-dependent shifts observed for the downfield resonance.

If the downfield resonance is assigned to xenon in reservoir III, these facts can be accounted for by a slow exchange dynamics. We consider it more likely that the downfield resonance is due to xenon, in both reservoirs III and IV, where occupancy of reservoir IV is increasingly favored as the temperature is lowered. The resulting weak exchange (due to low occupancy) between reservoirs II and III barely affects the shifts and relaxation times of xenon in reservoir II. Xenon atoms, however, in reservoir IV give rise to very large chemical shifts brought about by their spatial confinement. Therefore, we expected to observe only very weak evidence of exchange between the two resonances in a two-dimensional experiment.

Indeed, up to a mixing time of 10 ms for the carbon nanotubes oxidized with permanganate, no cross-peaks between the two ^{129}Xe NMR resonances were observed (Figure 7). Due to the longer T_1, a longer time scale could be probed for xenon in contact with the air-oxidized sample. This experiment was carried out on the sealed sample at a temperature of 215 K, where the signal-to-noise ratio was good for both resonances. For a mixing time of 300 ms, faint cross-peaks could be detected, indicative of only inefficient exchange between the two environments brought about by the low occupancy of reservoir III. It has been postulated for single-walled carbon nanotubes of 7.3 Å inner diameter that a quasi-one-dimensional xenon phase inside the tubes is in equilibrium with a two-dimensional gas phase on the outer surface.[18] We were not able to observe this exchange, which may be due to the different time scales probed. Moreover, the inner tube diameters of our carbon nanotubes were at least twice the diameter required for a one-dimensional phase. Further ^{129}Xe NMR experiments with single-walled carbon nanotubes are planned to elucidate this question. Because most of the signal intensity of the downfield resonance originates from xenon in reservoir IV, the increased line width under equilibrium conditions is probably brought about by the distribution of inner tube diameters ranging from 3 to 9 nm.[14] The contribution of chemical shift anisotropy to the line width must also be considered, due to the random orientation of the nanotubes. In this case, no effect of the gas flow rate on line width was expected because the gas flow rate does not change the population of randomly oriented sites with equal adsorption properties. In contrast, for a site heterogeneity, an effect of gas flow rate is conceivable: the strongest adsorption sites will most likely be populated. The nanotubes

(26) Jeener, J.; Meier, B. H.; Bachmann, P.; Ernst, R. R. *J. Chem. Phys.* **1979**, *71*, 4546−4553.

(27) Jameson, C. J.; Jameson, A. K.; Gerald, R. E., II; Lim, H.-M. *J. Phys. Chem. B* **1997**, *101*, 8418−8437.

(28) Chen, Q. J.; Fraissard, J. *J. Phys. Chem.* **1992**, *96*, 1814−1819.

(29) Torrey, H. C. *Phys. Rev.* **1963**, *130*, 2306−2312.

with the smallest diameter will give rise to the largest chemical shifts. If exchange between these sites is slow, the largest line width is expected under static conditions for which all sites are equally sampled, which is in agreement with the data. Slow site exchange is supported by the results from two-dimensional exchange NMR spectroscopy (Figure 7). Here, the peak for physisorbed xenon is elongated along the diagonal, which indicates no exchange between the different sites during the mixing time. As expected, these peaks became more rounded under conditions of observable exchange for the high xenon density sample.

The unique structure of carbon nanotubes raises the question about the diffusion mechanism of occluded gases. In addition to ordinary one-, two-, and three-dimensional diffusion, the possibility of single-file diffusion exists when the adsorbed atoms or molecules do not change their relative order during the observation time. Single-file diffusion gives rise to a change in the time-dependence of the mean particle displacement in comparison with ordinary diffusion.[30] Single-file diffusion has been observed, for example, with neutron scattering for cyclopropane in the channels of $AlPO_4$-5 with a channel diameter of 7.3 Å. Even though the carbon nanotubes investigated here have similarly large length-to-diameter ratios, the smallest internal tube diameter is still significantly larger than the diameter of a Xe atom (30 Å vs 4.4 Å). Although the diffusion coefficient of xenon under the experimental conditions applied is not known, an order-of-magnitude estimate can be made when comparing to the diffusion coefficient of xenon in a porous medium such as a zeolite. For a loading of one xenon atom per supercage, a diffusion coefficient D of 10^{-9} m^2 s^{-1} has been determined.[31] For ZSM-48, the diffusion coefficient for a small concentration of methane ($\theta = 0.11$) is 2.5×10^{-9} m^2/s at 155 K, but at a higher loading ($\theta = 0.48$) for single-file diffusion, the mobility factor is 2×10^{-12} m^2 s$^{-0.5}$.[30] Therefore, it is conceivable that, independent of the diffusion mechanism, xenon will be trapped in the interiors of the nanotubes once it has entered their interiors. With a length of about 50 μm and $D = 10^{-9}$ m^2 s^{-1}, it would take a Xe atom about 2.5 s to traverse a tube. This estimate is consistent with our assignment of the downfield resonance mainly originating from xenon in reservoir IV. Due to the very short relaxation time of xenon in contact with the permanganate oxidized sample, only a small fraction of the tube interior is sampled under optical-pumping conditions. Thus, the MnO_2 particles must be located within a few microns from the openings.

(30) Jobic, H.; Hahn, K.; Kärger, J.; Bee, M.; Tuel, A.; Noack, M.; Girnus, I.; Kearley, G. J. *J. Phys. Chem. B* **1997**, *101*, 5834−5841.

(31) Kärger, J.; Bar, N.-K.; Heink, W.; Pfeifer, H.; Seiffert, G. *Z. Naturforsch.* **1995**, *50a*, 186−190.

Conclusions

Different oxidation procedures for multiwall carbon nanotubes leave a distinct signature on the ^{129}Xe NMR chemical shift and ^{13}C and ^{129}Xe spin−lattice relaxation times. Residual paramagnetic MnO_2 particles contributed to the short spin−lattice relaxation times that were observed for the permanganate-oxidized sample, although other contributions such as chemical shift anisotropy or interaction with conduction electrons may also have been present. The thorough washing procedure should have removed all MnO_2 from the accessible sites which are in the interparticle space and on the outer surface of the nanotubes. Therefore, the interaction of xenon with the paramagnetic centers must arise from the interior of the tubes, which is in accordance with results from xenon sorption studies.[18] This conclusion is supported by the decrease in the chemical shift of the physisorbed xenon, as expected for xenon in confined spaces. This decrease alone, however, is not conclusive, because it would also be observed for shifts affected by interaction with paramagnetic species. Yet, the decrease in chemical shift is, likewise, detected for the diamagnetic, air-oxidized sample. Moreover, two-dimensional exchange NMR data of ^{129}Xe indicate slow exchange between different adsorption sites which are represented by nanotubes of different diameters. Because most of the xenon dwells in the interior of the tubes, only very inefficient exchange with xenon in the interparticle space was present. Occupancy of the interior of the nanotubes is strongly favored over the interparticle space and exterior adsorption sites when the temperature is lowered. This is an indication of strong adsorption sites in the tube interior: the Gibbs free energy must be dominated by the adsorption enthalpy, because the entropy of the system will most likely decrease upon xenon's occlusion by the nanotubes. In conclusion, our data strongly suggest that xenon and possibly other gases are readily trapped at low temperatures by multiwalled carbon nanotubes, which is important in light of nanotubes as potential gas storage media. ^{129}Xe NMR is a suitable technique to probe the interior of the tubes.

Acknowledgment. We acknowledge financial support through ACS-PRF Grant No. 30916-G and for an NMRPI grant through UCDRD of Los Alamos National Laboratory. The authors further acknowledge financial support through the Belgian Program on Inter-University Poles of Attraction initiated by the Belgian State, Prime Minister's Office for Scientific, Technical, and Cultural Affairs (OSTC-PAI-IUAP No. 4/10 on Reduced Dimensionality Systems), and the European Commission, TMR contract NAMITECH, ERBFMRX-CT96-0067 (DG12-MIHT). We also thank Dr. P. Grandinetti for free access to his program, RMN.

JA994441Y